Analysis of Heat Transfer and Flow Characteristics of a Helically Coiled Tube with Twisted Elliptical in a Low Reynolds Number Flow

Authors:

Jun Wang, Yaohui Liu, Ruoxi Ding

Date Submitted: 2023-02-21

Keywords: helically coiled tube, corrugated wall, heat transfer, flow characteristics, nanofluid

Abstract:

In this paper, the heat transfer and flow characteristics of a helically coiled tube with twisted elliptical in a low Reynolds number (Re = 500?3000) flow were investigated numerically. The working fluid flowed in a laminar regime. Numerical results were compared with empirical correlations in the existing literature, demonstrating the accuracy of the analysis in this study. Firstly, we investigated the effects of geometric parameters and Reynolds number on the heat transfer and flow characteristics. The results showed that lower twist pitch length and semi-major axis length could induce sufficient fluid mixing and a larger temperature gradient near the tube wall, enhancing the heat exchange and producing larger friction resistance. Overall, the heat transfer performances were improved by about 1.04?1.21 times and 1.02?1.23 times for different semi-major axis lengths and different twist pitch lengths, respectively, compared to the smooth helical coil. Secondly, by changing the working fluid, it was found that the Nu when oil was chosen as the working fluid was all 6?6.8 times higher than that of water. Moreover, the effect of using Al2O3 nanofluids with a concentration of 0.10 wt.%, 0.25 wt.% and 0.50 wt.% was discussed. It can be seen that the heat transfer capacity of nanofluids increased by approximately 2?18% compared to the reference model with water as the working fluid, and the nanofluid solution with higher concentration has better heat transfer performance. Finally, Nu and f correlations are given to predict the heat transfer and pressure drop in practical applications.

Record Type: Published Article

Submitted To: LAPSE (Living Archive for Process Systems Engineering)

Citation (overall record, always the latest version):	LAPSE:2023.0756
Citation (this specific file, latest version):	LAPSE:2023.0756-1
Citation (this specific file, this version):	LAPSE:2023.0756-1v1

DOI of Published Version: https://doi.org/10.3390/pr10112229

processes

MDPI

Article

Analysis of Heat Transfer and Flow Characteristics of a Helically Coiled Tube with Twisted Elliptical in a Low Reynolds Number Flow

Jun Wang *, Yaohui Liu and Ruoxi Ding

School of Power and Engineering, Jiangsu University of Science and Technology, Zhenjiang 212100, China
* Correspondence: ecsi-wj@163.com

Abstract: In this paper, the heat transfer and flow characteristics of a helically coiled tube with twisted elliptical in a low Reynolds number (*Re* = 500–3000) flow were investigated numerically. The working fluid flowed in a laminar regime. Numerical results were compared with empirical correlations in the existing literature, demonstrating the accuracy of the analysis in this study. Firstly, we investigated the effects of geometric parameters and Reynolds number on the heat transfer and flow characteristics. The results showed that lower twist pitch length and semi-major axis length could induce sufficient fluid mixing and a larger temperature gradient near the tube wall, enhancing the heat exchange and producing larger friction resistance. Overall, the heat transfer performances were improved by about 1.04–1.21 times and 1.02–1.23 times for different semi-major axis lengths and different twist pitch lengths, respectively, compared to the smooth helical coil. Secondly, by changing the working fluid, it was found that the *Nu* when oil was chosen as the working fluid was all 6–6.8 times higher than that of water. Moreover, the effect of using Al_2O_3 nanofluids with a concentration of 0.10 wt.%, 0.25 wt.% and 0.50 wt.% was discussed. It can be seen that the heat transfer capacity of nanofluids increased by approximately 2–18% compared to the reference model with water as the working fluid, and the nanofluid solution with higher concentration has better heat transfer performance. Finally, *Nu* and *f* correlations are given to predict the heat transfer and pressure drop in practical applications.

Keywords: helically coiled tube; corrugated wall; heat transfer; flow characteristics; nanofluid

Citation: Wang, J.; Liu, Y.; Ding, R. Analysis of Heat Transfer and Flow Characteristics of a Helically Coiled Tube with Twisted Elliptical in a Low Reynolds Number Flow. *Processes* **2022**, *10*, 2229. https://doi.org/10.3390/pr10112229

Academic Editor: Ireneusz Zbicinski

Received: 3 October 2022
Accepted: 26 October 2022
Published: 30 October 2022

1. Introduction

Nowadays, the sustainability of development continues to arouse people's attention, and energy efficiency is one of the main economic and technological challenges currently facing. A helically coiled tube heat exchanger, as one of the heat transfer enhancement techniques, has recently gained considerable attention, and it is widely used in various industrial applications as a key equipment for heat transfer and conversion [1,2]. In a heat exchanger, heat tends to be transferred from high-temperature fluid to low-temperature fluid through the tube walls. With the increase in flow resistance, energy efficiency is reduced. In order to achieve high energy conversion efficiency and effective energy-saving benefits, it is crucial to investigate heat exchange devices with higher heat transfer efficiency and lower pressure loss. For this reason, various convective heat transfer enhancement techniques have been developed in the past decades. The main methods included active enhancement [3–5], passive enhancement [6–8], and a combination of both [9,10].

Up to now, a number of researchers have conducted extensive experimental and theoretical studies to illustrate the heat transfer and flow characteristics of helically coiled tubes in laminar and turbulent flow regimes. Khoshvaght-Aliabadi et al. [11] compared and analyzed the thermal-hydraulic performance under three different geometric parameters (helical, spiral, and serpentine tubes). The results showed that the helical tube had the best performance compared with other tubes under the same geometry and operating conditions. Ammar Ali et al. [12] performed numerical simulations of the pressure drop

and heat transfer characteristics of smooth tubes and internal helical micro-finned tubes with two different fin height ratios, and they found that the heat transfer performance can be improved by using helical fin tubes and the optimal heat transfer can be achieved by optimizing the fin height ratio. Khoshvaght-Aliabadi and Feizabadi [13] numerically studied the forced convection heat transfer of laminar flow in a square spiral channel with corrugated side walls. They tested the corrugated structures on the upper, lower, inner and outer sides of the spiral channel as well as on the upper–lower and inner–outer sides, respectively. It was detected that the corrugations of each wall have different effects on the thermal and hydraulic characteristics of the helical coil. Promthaisong and Jedsadaratanachai et al. [14] numerically investigated the effects of depth ratio (e/D = 0.02–0.16), pitch ratio (p/D = 0.1–1.0), and Reynolds number (Re = 5000–20000) on the heat transfer flow characteristics of the fluid inside the spiral bellows. The results demonstrated that the influence of the bellows wall structure causes vortex flow, accelerates fluid mixing and improves heat transfer. Xin and Ebadian [15] experimentally investigated the hydrothermal properties of fluids in helical tubes with different geometrical parameters and Prandtl numbers. The experimental results show that the fluid flow and temperature field in the helical pipes were fully developed after two dimensionless distances (x/L), and the Nusselt number changed significantly at higher Prandtl numbers and Dean numbers.

In addition, some researchers have begun to focus on improving the heat transfer capability of helical coils through passive methods. Yu and Zhang et al. [16] numerically investigated the thermal-hydraulic performance of a twisted elliptical tube with three cross-sectional coils under turbulent conditions. They found that the average increase of Nu for the wire coils with circular cross-sections, square cross-sections and equilateral triangular cross-sections was 26%, 57% and 46%, respectively. Promvonge and Eiamsa-Ard [17] experimentally reported the heat transfer and flow characteristics in a circular tube fitted with conical-ring turbulators and a twisted-tape swirl generator. The results revealed that the smaller the twist ratio, the larger the heat transfer and friction factor at all Reynolds number conditions. And compared to using the conical-ring tube alone, the tube with the conical ring and twisted-tape provided approximately 4–10% of Nusselt value and 4–8% of heat transfer enhancement. Thianpong and Eiamsa-Ard et al. [18] conducted an experimental study of the friction and heat transfer behavior of fully developed turbulent flow in bellows fitted with a twisted tape swirl generator. The experimental results showed that the heat transfer coefficient and friction coefficient of bellows with twisted tape is higher than those of single corrugated pipe or plain pipe. Gkountas et al. [19] studied the thermal and hydraulic characteristics of a printed-circuit heat exchanger that uses Al_2O_3-water nanofluid as a precooler for the SCO_2 Brayton cycle. They found a 10% improvement in heat transfer coefficient compared to pure water as the working fluid, along with a 14% decrease in pressure drop. The use of nanofluids can have a positive effect on heat transfer enhancement.

As mentioned above, most of the existing research results discuss the influence of different geometric parameters and working fluids on the heat transfer performance of helical coils at a high Reynolds number, but the investigations at low Reynolds numbers are insufficient. The main purpose of this paper is to study the hydrothermal characteristics of helical coils with twisted elliptical (hereinafter referred to as HCTTE-tube) at low Reynolds number (Re = 500–3000). Numerical methods are used to understand the effects of different geometric parameters, Reynolds number and fluid properties of HCTTE tubes on heat transfer and flow resistance and to explain the heat transfer enhancement mechanism based on the distribution of velocity and temperature fields.

2. Model Description and Numerical Methodology

2.1. Physical Model

A three-dimensional computational model related to heat transfer and flow of HCTTE-tube was first developed. The physical model of the helically coiled tube is shown in Figure 1a. As shown in the figure, the main geometric parameters of the structure include

the helix diameter of the helically coiled tube (D), screw pitch (S), twist pitch along the main flow when the tube is twisted 180 deg (hereinafter referred to as twist pitch length, p). Considering the computational resources, the five-turn coil was considered in this study. Figure 1b shows the geometric details of the cross-sections, and the main parameters include the diameter of the tube (d), the semi-major axis (a), and the semi-minor axis (b). It should be mentioned here that Model 1 (hereinafter referred to as M1) and Model 2 (hereinafter referred to as M2) in Figure 1b have the same perimeter. M1 is used as a reference in this work. Equation (1) shows the calculation of perimeter (L), in the case of determining the diameter (d) and the length of the semi-major axis (a), the length of the semi-minor axis (b) is calculated by the Ramanujan formula. As given in Table 1, the study was carried out under four different lengths of semi-major axis (a = 4.4, 4.8, 5.2 and 5.6 mm) and four different lengths of twist pitch length (p = 35, 45, 55 and 65 mm). The helix diameter of the helically coiled tube (D) and screw pitch (S) is fixed at 90 mm and 30 mm, respectively. The values of the specific structural parameter ranges in the numerical simulation are shown in Table 1.

$$L = \begin{cases} \pi d \Rightarrow \text{M1} \\ \pi\left[3(a+b) - \sqrt{(3a+b)(a+3b)}\right] \Rightarrow \text{M2} \end{cases} \quad (1)$$

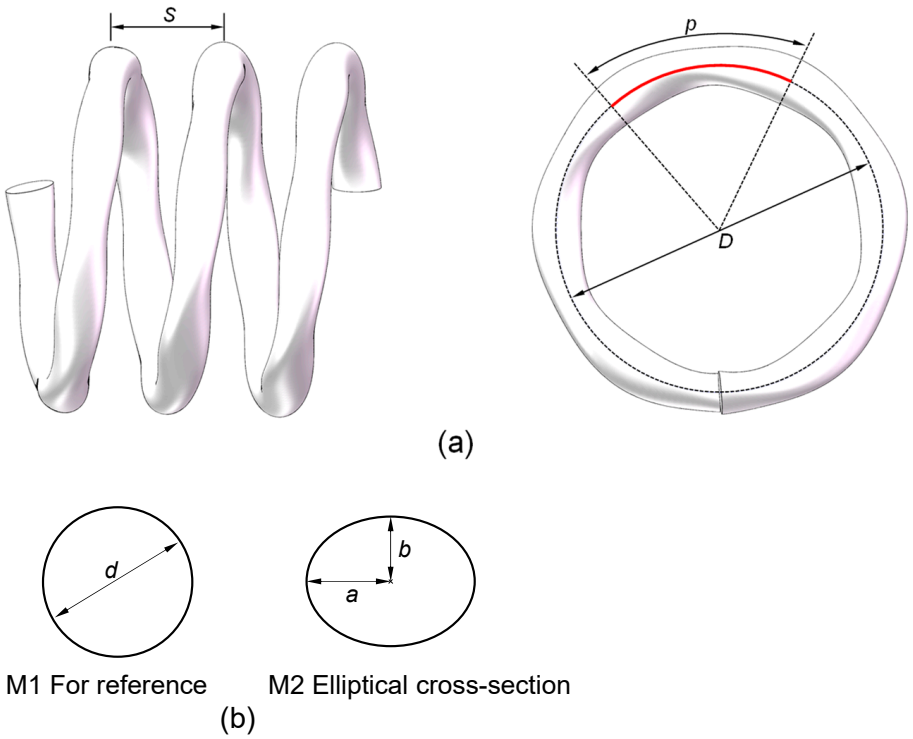

Figure 1. (**a**) Physical model of HCTTE-tube; (**b**) Geometrical details of the cross-sections.

Table 1. Specific structural parameter ranges.

D (mm)	*S* (mm)	*p* (mm)	*a* (mm)	*d* (mm)	*a*/*d*	*p*/*d*	*Re*
90	30	35	4.4	12	0.3667	2.9167	500–3000
90	30	45	4.8	12	0.4000	3.7500	500–3000
90	30	55	5.2	12	0.4333	4.5833	500–3000
90	30	65	5.6	12	0.4667	5.4167	500–3000

2.2. Governing Equations

In this paper, the heat transfer performance and flow characteristics of the HCTTE tube were investigated numerically in the Reynolds number range of 500–3000. Flow is considered incompressible, steady state, homogeneous and Newtonian with the negligible effect of viscous heating. The working fluid is atmospheric pressure water, and the temperature is uniform when entering the tube. Table 2 shows some of the physical properties of water, assuming a constant thermophysical property with a Prandtl number of 6.99.

Table 2. Properties of the working fluid (water).

Density (kg m^{-3})	c_p Specific Heat Capacity (J Kg^{-1} K^{-1})	Thermal Conductivity (W m^{-1} K^{-1})	Dynamic Viscosity (Pa s)	*Pr*
998.2	4183	0.6	0.001003	6.99

Schmidt [20] reported the correlation equation for the critical Reynolds number in the coiled tube:

$$Re_{cr} = 2300\left[1 + 8.6\left(\frac{d}{D}\right)^{0.45}\right] \quad (2)$$

Srinivasan et al. [21] summarized the equation for evaluating the critical Reynolds number of a helical coil:

$$Re_{cr} = 2100\left(1 + 12\sqrt{\frac{d}{D}}\right) \quad (3)$$

The range of Reynolds numbers considered in this work is far below the reference critical Reynolds number, so the flow is considered to be laminar.

In order to simplify the numerical model, the following assumptions are adopted:

(1) The physical property parameters of the working fluid are determined according to the temperature of the working fluid;
(2) Thermal radiation, the effects of gravity, natural convection and viscous dissipation are neglected;
(3) The thickness of coiled tubes is neglected.

The governing equations of velocity field and temperature distribution are as follows:

Continuity equation:

$$\frac{\partial}{\partial x_i}(\rho u_i) = 0 \quad (4)$$

Momentum equation:

$$\frac{\partial}{\partial x_j}(\rho u_i u_j) = -\frac{\partial P}{\partial x_i} + \frac{\partial}{\partial x_j}\left[\mu\left(\frac{\partial u_i}{\partial x_j} + \frac{\partial u_j}{\partial x_i}\right)\right] \quad (5)$$

Energy equation:

$$\frac{\partial}{\partial x_i}(\rho c_p u_i T) = \frac{\partial}{\partial x_i}\left(\lambda\frac{\partial T}{\partial x_i}\right) \quad (6)$$

where ρ, u, P, T, μ, c_p and λ are the fluid density, velocity, pressure, temperature, dynamic viscosity, specific heat capacity, and thermal conductivity.

2.3. Boundary Conditions

The boundary conditions were set as follows: the inlet of the working fluid was set as the velocity inlet, the inlet temperature was fixed at 293.15 K, and the inlet velocity was calculated according to the Reynolds number. Under appropriate reflow conditions, the outlet was set to the pressure outlet and the relative pressure was set to zero. No-slip boundary conditions were used for fluid velocity on the wall, and the tube wall temperature was constant at 353.15 K.

2.4. Numerical Procedure

In this work, the control volume method was used to solve the governing equations with boundary conditions through the CFD software ANSYS FLUENT. The coupling of the pressure field and velocity components was solved using the Semi-Implicit-Pressure-Linked Equation (SIMPLE) algorithm. Furthermore, the PRESTO scheme was chosen to correct the pressure equation. The second-order upwind scheme was chosen to solve the momentum and energy equations. The relaxation factors of pressure, velocity and energy were set to 0.3, 0.6 and 1, respectively. In addition, the convergence criterion for the energy conservation equation was set to 10^{-8}, and the convergence criterion for the remaining residuals was set to 10^{-6}.

2.5. Parameter Definition

The relationship between the inlet velocity and the Reynolds number Re is defined as follows:

$$Re = \frac{d_e u_{in} \rho}{\mu} \tag{7}$$

where d_e is the tube side hydraulic diameter, as below:

$$d_e = \frac{4A}{Pe} \tag{8}$$

where the A is the cross-sectional area, and the Pe is the wetted perimeter.

The Nusselt number Nu can be calculated as:

$$Nu = \frac{hd_e}{\lambda} \tag{9}$$

where λ is the thermal conductivity, h is the heat transfer coefficient:

$$h = \frac{Q}{A \cdot \Delta T_m} = \frac{m \cdot c_p (T_{out} - T_{in})}{A \cdot \Delta T_m} \tag{10}$$

where T_{in} and T_{out} are the inlet and outlet temperatures, respectively. Q is the convection heat transfer rate, m is the mass flow rate, and A is the heat transfer area. ΔT_m is the logarithmic mean temperature difference, which can be calculated by:

$$\Delta T_m = \frac{(T_{wall} - T_{in}) - (T_{wall} - T_{out})}{\ln \frac{T_{wall} - T_{in}}{T_{wall} - T_{out}}} \tag{11}$$

where T_{wall} denotes the wall temperature.

The friction factor f is attained as follows:

$$f = \frac{2 \Delta P d_e}{\rho u^2 L} \tag{12}$$

where u is the average velocity of the fluid, ΔP represents the pressure drop as below:

$$\Delta P = P_{in} - P_{out} \tag{13}$$

In this paper, a single-phase mixing model is used to study the heat transfer and flow of Al_2O_3 nanofluid as working fluid. According to a previous report by Ho and Pan [22]. The governing equation of the two-dimensional motion of Al_2O_3 nanofluid is as follows:

The density of nanofluids:

$$\rho_{nf} = \varphi \rho_p + (1 - \varphi) \rho_{bf} \tag{14}$$

where φ is the volume fraction of nanoparticles.

The thermal conductivity of nanofluids:

$$\frac{k_{nf}}{k_{bf}} = \frac{k_p + 2k_{bf} - 2\varphi\left(k_{bf} - k_p\right)}{k_p + 2k_{bf} + \varphi\left(k_{bf} - k_p\right)} \tag{15}$$

The dynamic viscosity of nanofluids:

$$\mu_{nf} = \mu_{bf} \frac{1}{(1-\varphi)^{2.5}} \tag{16}$$

2.6. Comprehensive Evaluation Criteria

In this study, the Thermal Performance Factor TPF was used to evaluate the effect of heat transfer enhancement in HCTTE-tube. Typically, heat transfer enhancement comes at the expense of additional frictional dissipation of energy. A typical research method is: under constant pumping power, compare the heat transfer and pressure drop consumption between HCTTE-tube and a smooth helically coiled tube, which is defined as:

$$TPF = \frac{h/h_s}{(\Delta P/\Delta P_s)^{1/3}} \tag{17}$$

where h and ΔP are the heat transfer coefficient and pressure drop for HCTTE-tube, respectively, h_s and ΔP_s are the corresponding values for smooth helical coil, respectively, evaluated at the same Re value. It is worth noting that the ΔP and ΔP_s are adopted instead of f and f_s to eliminate the effect of different d_e.

2.7. Mesh Generation and Independence Test

The quality of the mesh in the computational domain determines the stability and accuracy of the numerical simulation. The mesh system employed in this study was generated using the commercial software ANSYS Mesh. Unstructured grids were generated in the fluid flow area, and the local grids were refined considering the flow characteristics of the boundary layer region. The Orthogonal Quality of the overall grid was greater than 0.8 and the Skewness was less than 0.2, which indicates the grid quality was good.

To ensure the reliability of the numerical results, grid-independent verification was conducted after meshing. Taking HCTTE-tube with p = 45 mm and a = 5.2 mm as an example, the simulation models with six grid systems were studied. Figure 2 shows the changing situation of Nu and f with different grid sizes under the Re = 1500. As depicted in Figure 2, when the grid number is more than 3.1 million elements, Nu and f tend to be a fixed values, and the error is also controlled within a very small range. Thus, considering the solution time and convergence accuracy of the model, 3.1 million grids were sufficient for simulation calculation.

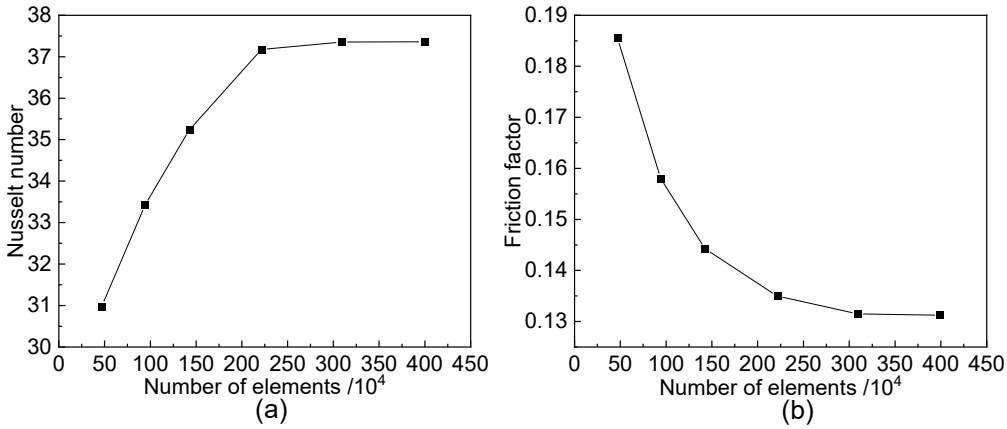

Figure 2. The Nusselt number and friction factor with different grid systems. (**a**) Nusselt number; (**b**) friction factor.

3. Results and Discussion

3.1. Model Validation

In order to verify the accuracy of the numerical solution method, the Nu and f that characterize the heat transfer performance of the helically coiled tube calculated by

the simulation were compared with the results available in the literature. Since it was difficult to find experimental data with the same geometrical conditions as the present work, the results of a spiral coil with a circular cross-section were chosen for verification. The correlations used in the validation are shown in Table 3 and the comparison results are shown in Figure 3. It is observed that the calculated Nu and f are between the two empirical, theoretical values, and there is good agreement between the present simulations and the theoretical values. Furthermore, the relative errors between simulation results and the experimental experience values of Nu and f are within the allowable range of the project. In summary, the simulation results of this work are considered to be reliable and accurate.

Table 3. Different correlations for Nusselt number and friction factor in helical coils.

Reference	Correlation	Validity Range
Xin and Ebadian [15]	$Nu = \left(2.153 + 0.318De^{0.643}\right)Pr^{0.177}$	$20 < De < 2000$, $0.7 < Pr < 175$
Salimpour [23]	$Nu = 0.152De^{0.431}Pr^{1.06}\gamma^{-0.277}$	$De < 3000$
Yanase et al. [24]	$\frac{f_c}{f_s} = 0.557 + 0.0938De^{0.5}$	Laminar flow
Itō [25]	$\frac{f_c}{f_s} = 21.5De/\left(1.56 + \log_{10} De\right)^{5.73}$	Laminar flow, $13.5 < De < 2000$

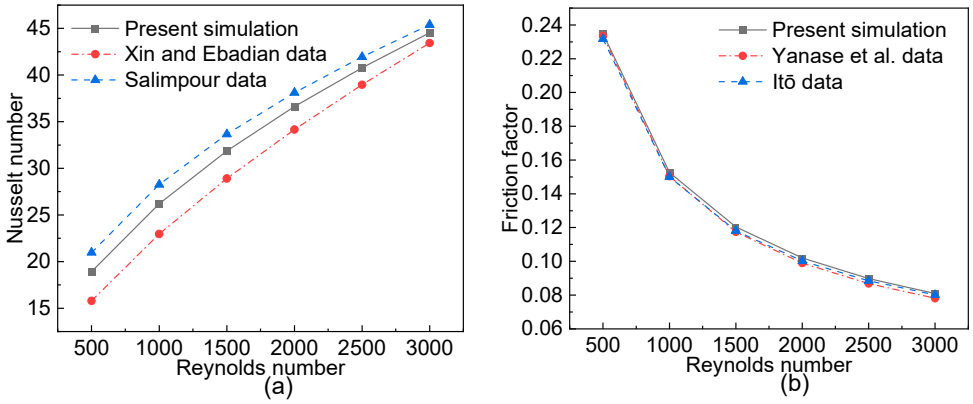

Figure 3. Comparison results of Nusselt number and friction factor. (**a**) Nusselt number; (**b**) friction factor.

In this work, the variations of screw pitch on the heat transfer and flow of the HCTTE-tube were not specifically investigated. Several studies [26,27] have reported this problem, i.e., no sensitive change in Nu and f by changing the coil pitch.

3.2. Comparison of HCTTE-Tube and Smooth Helically Coiled Tube

To further investigate the effect of structural parameters on the heat transfer and flow characteristics of the HCTTE-tube, the flow heat transfer mechanism at Re = 1500 is analyzed by comparing HCTTE-tube (p = 45 mm and a = 5.2 mm) with a smooth helically coiled tube.

Figure 4 presents the streamlines, vectors and temperature distributions at the same position slice for both structures. It is worth noting that in HCTTE-tube, a secondary flow is generated in a plane perpendicular to the direction of fluid flow, and these periodic corrugated wall structures make the streamlines completely disordered, which significantly affects the velocity and vector of the passing fluid. In the reference model, the streamlines are roughly parallel in the direction of flow. Also, compared to the reference model, two very significant vortices are generated in HCTTE-tube, which have a direct impact on the flow and temperature field distribution inside the tube. The presence of this enhanced vortex raises the mixing temperature inside the tube and increases the heat transfer, which ultimately manifests itself in a more uniform temperature distribution.

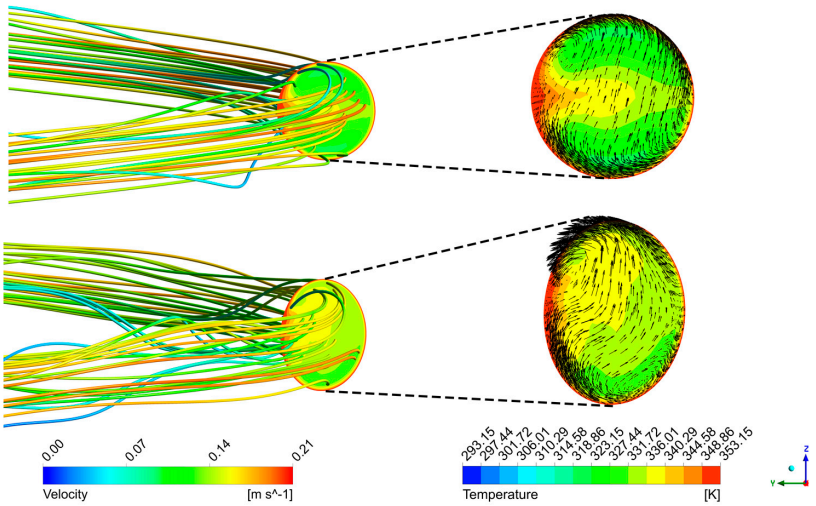

Figure 4. Effects of corrugated structures on streamlines, velocity contours, and vectors at p = 45 mm, a = 5.2 mm, and Re = 1500.

Figure 5 shows the velocity field at each circulation cross-section of the HCTTE-tube from the inlet to the outlet. It can be clearly seen that due to the presence of centrifugal forces, the secondary flow pushes the working fluid to the outer region, so that the outer side of the helical coil obtains a larger velocity, resulting in a much larger velocity gradient near the outer wall of the tube than the inner wall. In addition, this secondary flow can affect the heat transfer mechanism, and the corrugated wall structures of the HCTTE-tube disrupt the regular velocity distribution compared to the saddle velocity contours in the circulation cross-section of the reference model, which in turn intensifies the heat transfer effect.

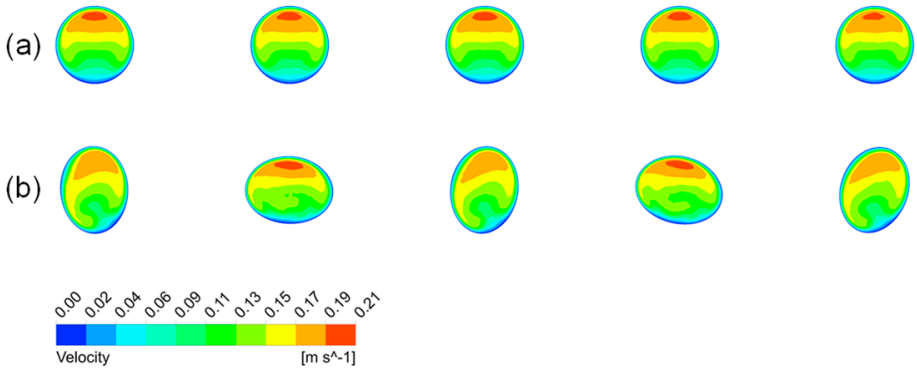

Figure 5. The velocity fields of each cycle cross-section from the inlet to the outlet (**a**) Smooth helically coiled tube; (**b**) HCTTE-tube.

Figure 6 depicts the temperature field of the entire longitudinal section at Re = 1500. As can be seen from the figure, the temperature of HCTTE-tube is higher than that of the reference model at the same transverse position, with a significant heat transfer advantage. And under the same cross-sectional perimeter, the outlet temperature of HCTTE-tube is higher than that of the smooth helical coil.

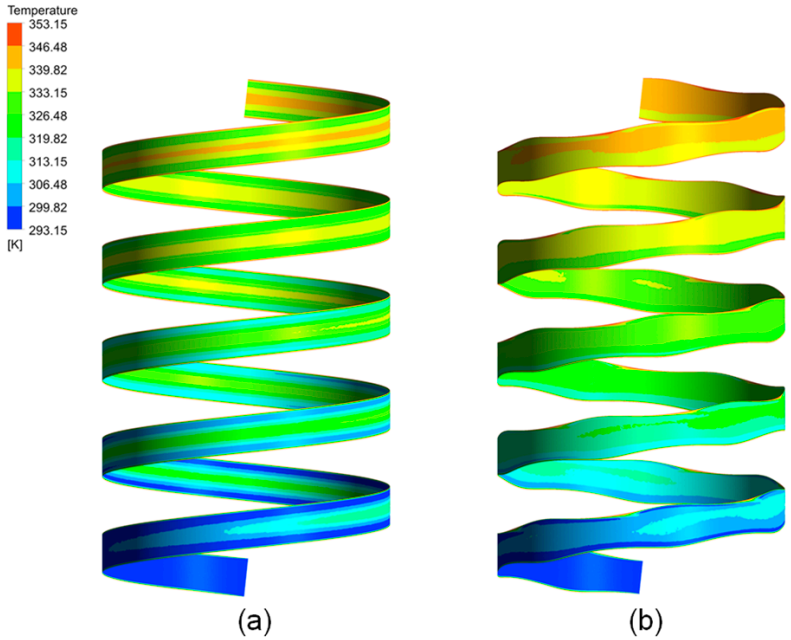

Figure 6. The temperature fields of longitudinal section (*Re* = 1500) (**a**) Smooth helically coiled tube; (**b**) HCTTE-tube.

3.3. Influences of the Semi-Major Axis Length (a) on Flow and Heat Transfer

Figure 7 shows the temperature contours within each circulation section from the inlet to the outlet for the smooth helical coil and HCTTE-tube with different semi-major axis lengths at *Re* = 1500. It can be seen that, compared with the reference model, the fluid temperature distribution in the tube is more uniform due to the flow mixing caused by the corrugated wall structure of the HCTTE-tube.

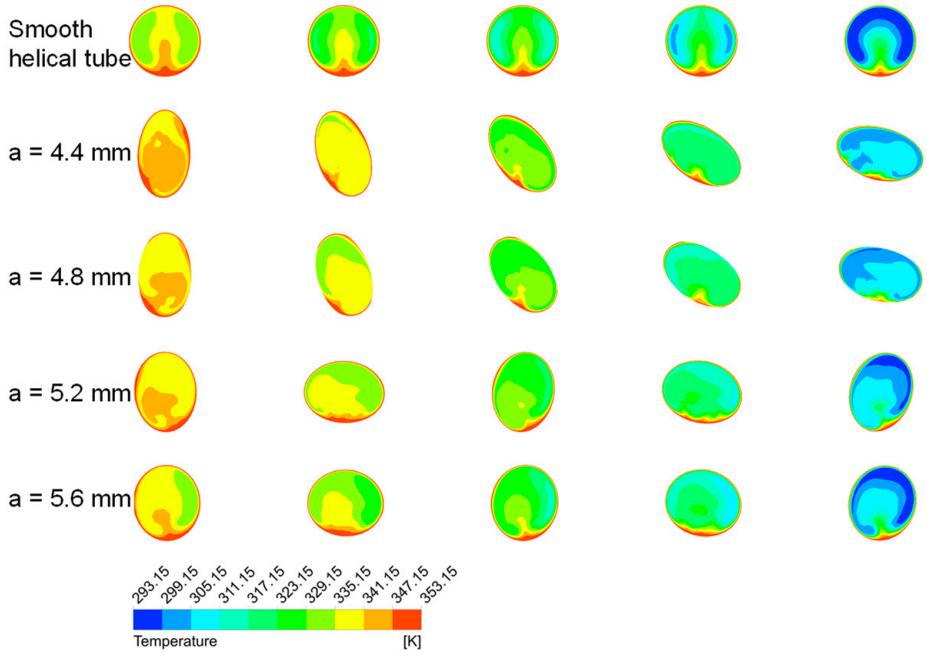

Figure 7. Temperature contours for different semi-major axis lengths (*Re* = 1500).

Moreover, it is observed that in the case of a = 4.4 mm, the mixing of the fluid is better at the selected cross-section, and the overall average temperature is greater than the other structures. This is because more powerful swirl flow can be generated when the s semi-major axis length is smaller, bringing stronger flow perturbation and thus significantly increasing the velocity gradient near the boundary layer, enhancing the heat transfer effect.

The variations of Nu and f with the increase of Reynolds number under different semi-major axis lengths are shown in Figure 8a,b, respectively. It is found that the Nu increases with the decreasing of semi-major axis lengths and the increasing of Reynolds numbers, and the f decreases with the increasing of semi-major axis lengths and Reynolds numbers. The corrugated wall structures can enhance the Nu of the HCTTE-tube, resulting in the overall thermal performance being improved. In the case of different semi-major axis lengths, the heat transfer performance is improved by about 1.04–1.21 times compared to the reference model. The reason may be that, due to the effect of secondary flow, the fluid velocity changes rapidly in the radial cross-sectional location of the coil, resulting in a better mixing between the hot region near the wall and the cold region in the center, which makes the temperature distribution more uniform. However, in HCTTE-tube, the reduction of the semi-major axis length results in higher pressure drop values. As can be seen from the figure, the f with semi-major axis lengths of 4.4, 4.8, 5.2 and 5.6 mm increase almost 114%, 112%, 109% and 103% compared to the reference model. It can be explained that when the semi-major axis length decreases, the blockage effect increases, resulting in an increase in the friction factor.

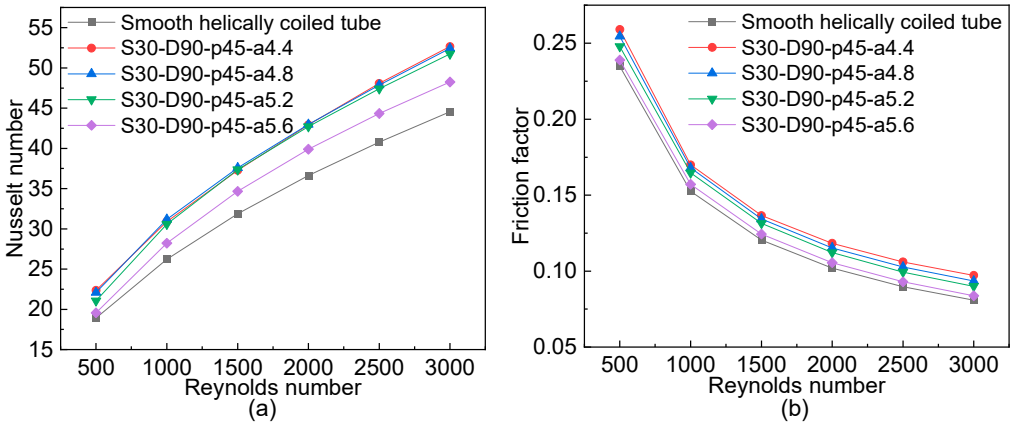

Figure 8. The variations of Nusselt number and friction factor with Reynolds number of different semi-major axis lengths. (**a**) Nusselt number; (**b**) friction factor.

$TPF > 1$ indicates that the enhancement of heat transfer performance is more advantageous than the pressure loss. Figure 9 shows the variation of the TPF with the length of the semi-major axis at different Reynolds numbers. In the figure, all corrugated structure models have thermal performance factors higher than 1, and the thermal performance factors of all models first increases and then decreases with the increase of Reynolds number, with optimal values obtained at Re = 1000 or 1500. This is due to the fact that when $Re > 1000$, the pressure loss in the fluid flow through the HCTTE-tube increases significantly, outweighing the improvement in heat transfer. Among the tested structural parameters, when a = 4.8 mm and Re = 1000, the maximum thermal performance factor can reach 1.19.

3.4. Influences of Twist Pitch Length (p) on Flow and Heat Transfer

In this section, the effect of twist pitch length on heat transfer and pressure drop in HCTTE-tube is mainly explained. In order to make a good comparison between the various models, Figure 10 presents the temperature distribution in the cross-section ($y < 0$) of the smooth helical coil and HCTTE-tube with different twist pitch lengths at Re = 1500. Compared with the reference model, there is mixed flow in the HCTTE-tube and the temperature distribution is more uniform. In addition, the temperature is lower in some

parts of the cross-section and higher in other parts, which indicates that the swirl flow caused by the twisting of the coil has a significant effect on the temperature field.

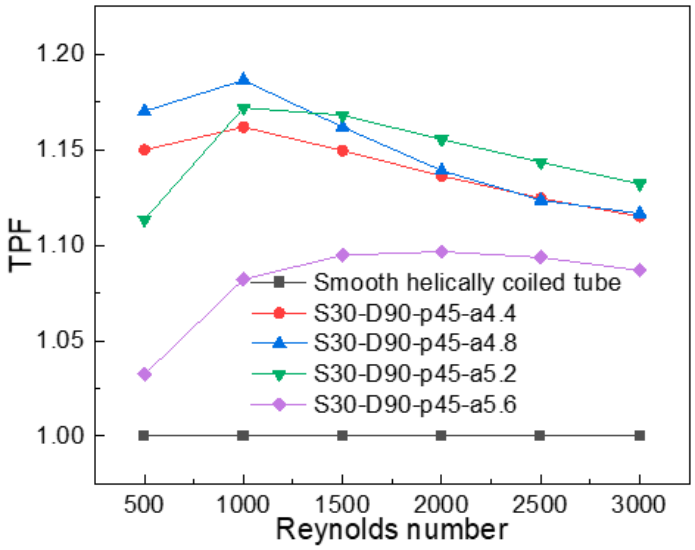

Figure 9. The variations of *TPF* with the length of the semi-major axis at different Reynolds numbers.

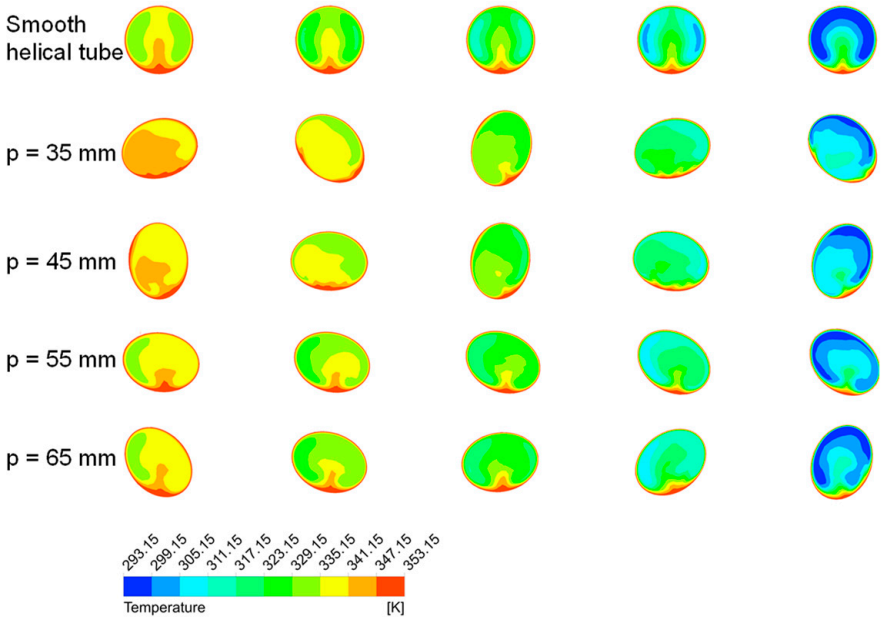

Figure 10. Temperature contours for different twist pitch lengths (*Re* = 1500).

In selected cross-sections, it can be found that the area of the high-temperature region increases with decreasing twist pitch length. The temperature contour of p = 35 mm shows that the swirl flow at a smaller twist pitch length can break the boundary layer more effectively and create a larger temperature gradient near the tube wall, which facilitates a more adequate mixing of the fluid.

Four different twist pitch lengths of 35, 45, 55 and 65 mm in six Reynolds numbers were tested for a = 5.2 mm to see the effects on heat transfer and flow characteristics. The results in Figure 11 show that the Nu increases with increasing Reynolds number, while the f decreases. Also, the relative Nu increases with increasing Reynolds number, and smaller twist pitch length is more effective at high Reynolds numbers. For all tested HCTTE-tube, the heat transfer performance can be improved by 1.16–1.29 times when Re = 3000. At a lower Reynolds number, the f increases by about 1–9% by the decrease of twist pitch

length from 65 mm to 35 mm, while at higher Reynolds number, the f increases by about 1–25% under the same conditions. This may be related to the fact that the streamlines become tortuous as the Reynolds number increases, which results in a higher temperature gradient. As the twist pitch length gradually decreases, the flow velocity increases in the normal plane of the main flow direction, which is more conducive to increasing the mixed flow, making the temperature distribution more uniform. It is obvious that for the same length of HCTTE-tube, reducing the twist pitch can increase the number of corrugated structures, resulting in a larger windward area in the mainstream direction, which increases the pressure drop inside the tube.

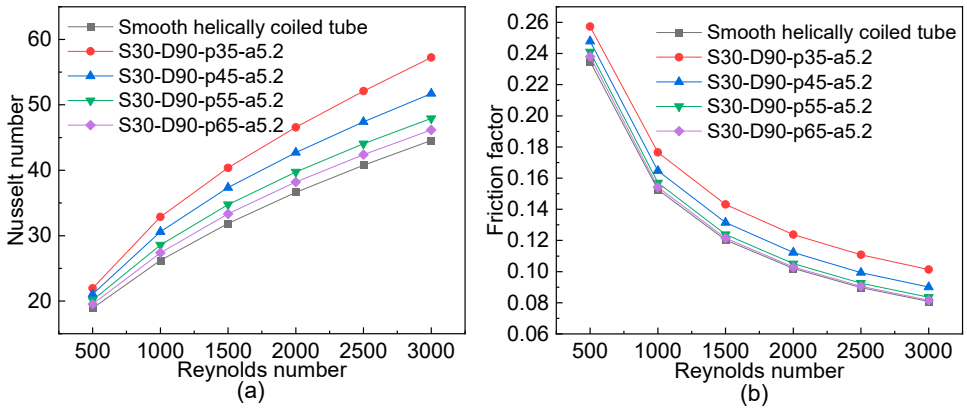

Figure 11. The variations of Nusselt number and friction factor with Reynolds number of different twist pitch lengths. (**a**) Nusselt number; (**b**) friction factor.

Figure 12 shows the variation of TPF with the different twist pitch lengths at different Reynolds. It can be seen that the overall hydrothermal performance of all tested models is better than the reference model. In addition, the TPF increases with the increase of Reynolds number until about Re = 1000. The opposite trend occurs when Re > 1000 because the friction factor increases faster than the Nusselt number. It is worth noting that the thermal performance factor of HCTTE-tube with different twist pitch lengths range from 1.05 to 1.23 at Re = 1000.

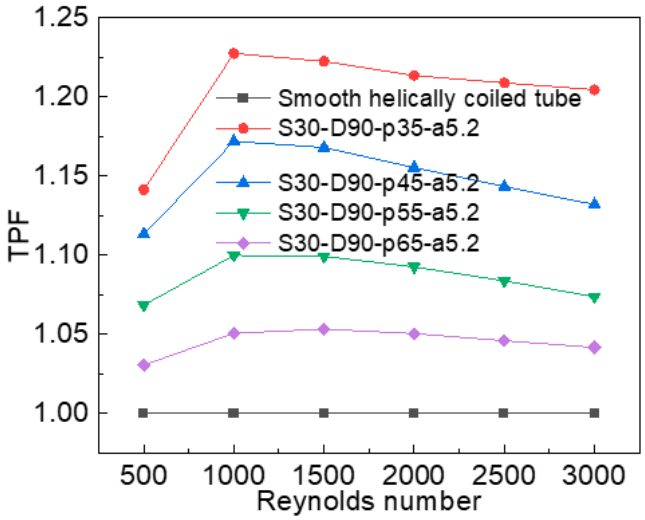

Figure 12. The variations of TPF with Reynolds number of different twist pitch lengths.

Figure 13 illustrates the 3D graphs to evaluate the synergistic effect of the semi-major axis length (a) and twist pitch length (p) on the hydrothermal properties of the HCTTE-tube at Re = 1500. It can be perceived that when p takes the minimum value, and 4.4 mm < a < 5.0 mm, the Nusselt number can reach the maximum value; p and a take the

maximum value at the same time, the friction factor meets a minimum level. For the *TPF* value, it is obvious that the maximum thermal performance can be obtained when the maximum Nusselt number and the minimum friction coefficient are reached. As can be seen from Figure 13c, when p takes the minimum value, and 4.8 mm < a < 5.1 mm, *TPF* can reach the maximum value.

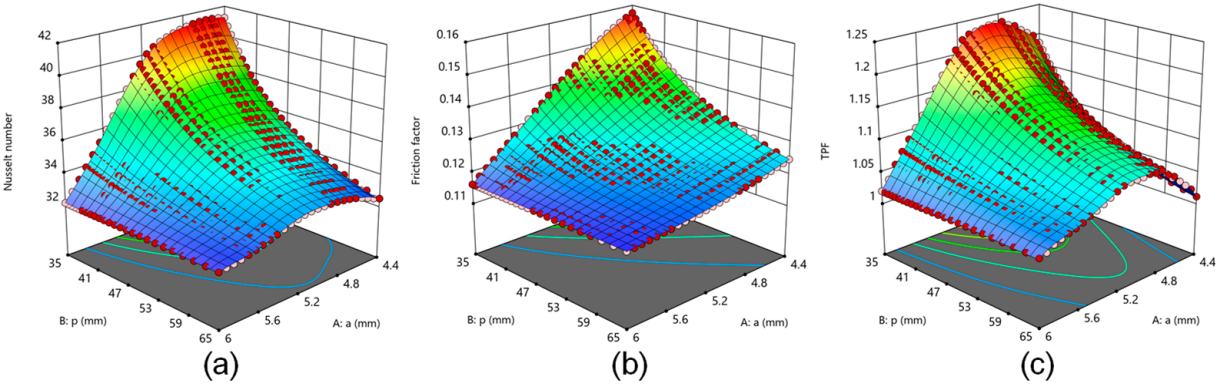

Figure 13. Response surface of the semi-major axis length and twist pitch length on objectives. (**a**) the synergistic effect of a and p on *Nu*; (**b**) the synergistic effect of a and p on f; (**c**) the synergistic effect of a and p on *TPF*.

3.5. Influences of Prandtl Number on Flow and Heat Transfer

In the case of boundary layer flow, the Prandtl number is related to the velocity boundary layer thickness and thermal boundary layer thickness. When the Prandtl number increases, the kinematic viscosity of the working fluid increases and thus, the flow velocity inside the HCTTE-tube will be higher, resulting in a decrease in the thickness of the thermal boundary layer and an increase in the temperature gradient. In this study, simulations were performed using ethylene-glycol (Pr = 150.46) and engine-oil (Pr = 1965) as additional fluids, and the results obtained were compared with water. Figure 14 shows the variation of Nu and f with Reynolds number for three working fluids. The results showed that the Nusselt number increases with the increase of the Reynolds number when using ethylene-glycol or engine oil as the working fluid, while the friction factor shows the opposite trend, which verifies the analysis results when water is used as the working fluid. It is worth noting that in all tests, the Nusselt number when engine oil is chosen as the working fluid is 6–6.8 times higher than that of water, but the change in friction factor is not significant.

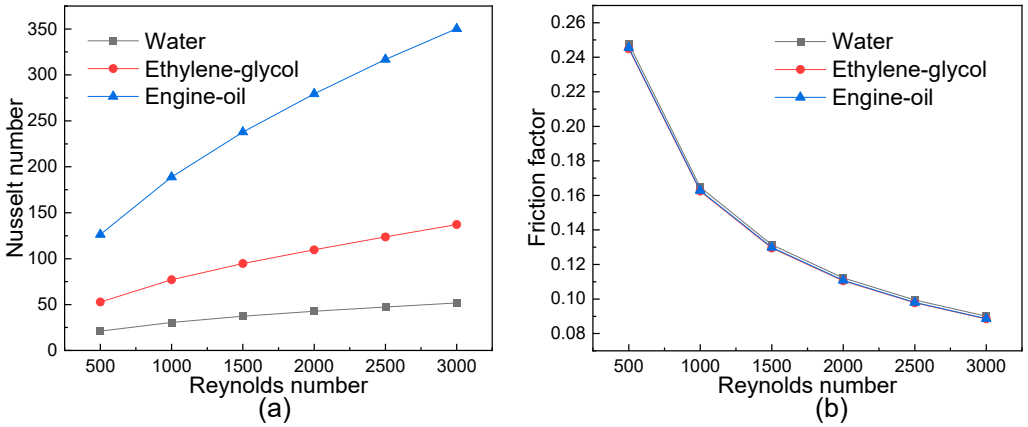

Figure 14. Effect of Prandtl number at p = 45 mm and a = 5.2 mm. (**a**) Nusselt number; (**b**) friction factor.

3.6. Effect of Using Nanofluid

In this part, Al_2O_3 nanofluid is used as the working fluid to simulate the hydrothermal performance of HCTTE-tube (p = 45 mm, a = 5.2 mm) under different Reynolds numbers. The variation of nanofluid with different mass fractions and Reynolds number is shown in Figure 15. It can be seen that the nanofluid as a working fluid has better heat transfer performance compared to water. And at the same Reynolds number, Nu and f increase with the increase of nanofluid concentration.

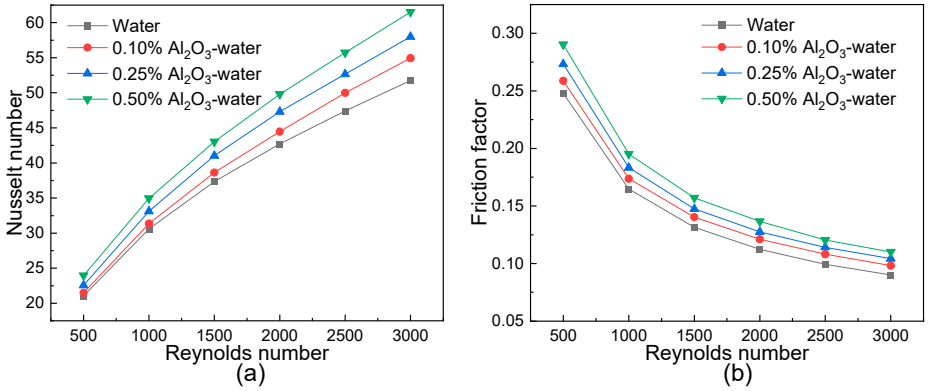

Figure 15. Nusselt number and friction factor corresponding to different volume concentrations in HCTTE-tube. (**a**) Nusselt number; (**b**) friction factor.

In this study, the heat transfer capacity of nanofluids increased by approximately 2–18% compared to water. This can be attributed to the fact that the thermal conductivity of the nanoparticles in nanofluid is much higher than that of the single base fluid (water), leading to higher energy exchange. In addition, the viscosity increases when the concentration of nanofluid increases, resulting in a greater resistance to the flow of the fluid. Therefore, at any Reynolds number, the friction factor of water as a working fluid is lower than that of nanofluid under corresponding conditions.

4. Correlations

In this study, the effect of the variation of geometric model parameters, Reynolds number and Prandtl number on the heat transfer and flow characteristics of the proposed HCTTE-tube were investigated. On the basis of the data obtained from all tests, the criterion correlation between Nu, f of HCTTE-tube and multiple variables was obtained. MATLAB software was used for multiple linear regression analysis. These fitted correlations take the following form:

$$Nu = 0.66275Re^{0.50508}Pr^{0.32743}\left(\frac{a}{b}\right)^{-0.19620}\left(\frac{p}{d}\right)^{-0.28430} \quad (18)$$

$$f = 10.93348Re^{-0.56554}Pr^{-0.00255}\left(\frac{a}{b}\right)^{-0.24335}\left(\frac{p}{d}\right)^{-0.25628} \quad (19)$$

The determination coefficient R^2 of the Nusselt number correlation is 0.99801, and 0.99663 for the friction factor correlation. It should be mentioned that the value d (12 mm) is the diameter of a circle of equal circumference to the cross-section of HCTTE-tube in the simulations. Figure 16 compares the correlation between predicted data and simulated results. It can be seen that the deviation between the two types of data is less than 10%. This indicates that the criterion correlations for characterizing the heat transfer and flow characteristics in HCTTE-tube are reliable and appropriate.

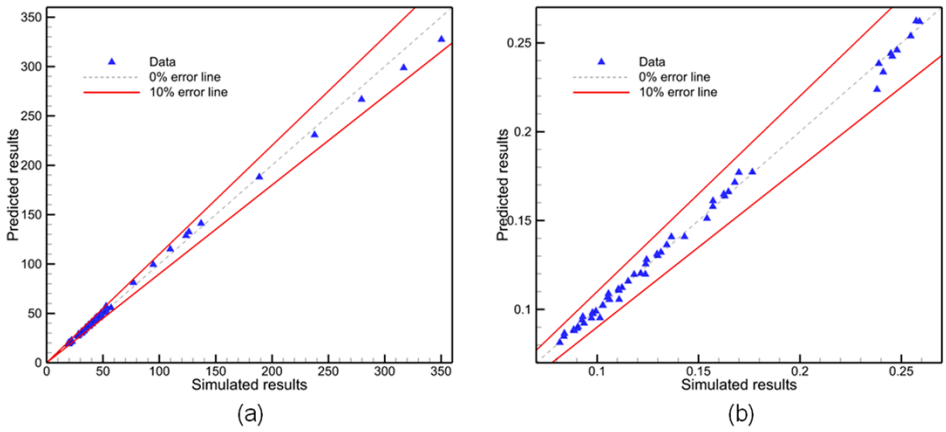

Figure 16. The comparison of Nusselt number and friction factor between predict result and simulation result: (**a**) Nusselt number (**b**) friction factor.

5. Conclusions

In this work, the heat transfer and flow characteristics of a helically coiled tube with a twisted elliptical were studied and discussed by using computational fluid dynamics method. Reynolds numbers in all simulations ranged from 500 to 3000, and the flow was laminar. Firstly, keeping the helix diameter and screw pitch of HCTTE-tube constant, the effects of semi-major axis length and twist pitch length on Nusselt number, friction factor and thermal performance were investigated at different Reynolds numbers, respectively. The effect of the Prandtl number is then illustrated by using ethylene-glycol and engine-oil as working fluids. Finally, the enhanced heat transfer performance of Al_2O_3 nanofluids was discussed. The main conclusions are drawn as follows:

Compared with the smooth helical coil, HCTTE-tube can provide higher heat transfer. Its corrugated wall structures increase the mixing flow of the fluid inside the tube and make the temperature distribution more uniform. But under the same conditions, a higher value of pressure drop will be generated due to the blockage effect of the flow channel.

At constant Reynolds number, the Nusselt number and friction factor increase with decreasing semi-major axis length and twist pitch length. Overall, HCTTE-tube has better hydrothermal performance compared to a smooth helical coil.

It can be observed that at the same Reynolds number, the Nusselt numbers of ethylene-glycol and engine-oil are higher than those of base fluid, but the effect on the friction factor is not significant.

Compared with water as the working fluid, nanofluid has better heat transfer enhancement performance.

The criterion correlations of heat transfer and flow in the HCTTE-tube were proposed, and its reliability and applicability were verified.

Author Contributions: Conceptualization, J.W.; Formal analysis, J.W. and Y.L.; Investigation, R.D.; Methodology, Y.L.; Project administration, J.W.; Software, Y.L. and R.D.; Supervision, J.W.; Validation, Y.L.; Visualization, Y.L.; Writing—original draft, Y.L.; Writing—review & editing, J.W. All authors have read and agreed to the published version of the manuscript.

Funding: This research received no external funding.

Conflicts of Interest: The authors declare that they have no known competing financial interests or personal relationships that could have appeared to influence the work reported in this paper.

Nomenclature

A	heat transfer area (m^2)
L	perimeter (mm)
D	helix diameter of helically coiled tube (mm)
S	screw pitch (mm)
p	twist pitch along the main flow when tube is twisted 180 deg (mm)
d	diameter of tube (mm)
a	the semi-major axis (mm)
b	the semi-minor axis (mm)
d_e	hydraulic diameter (mm)
c_p	specific heat capacity (J kg^{-1} K^{-1})
f	friction factor, dimensionless
h	heat transfer coefficient (W m^{-2} K^{-1})
m	mass flow rate (kg s^{-1})
Nu	Nusselt number, dimensionless
Pr	Prandtl number, dimensionless
Re	Reynolds number, dimensionless
Re_{cr}	critical Reynolds number
Pe	wetted perimeter (mm)
P	pressure (Pa)
ΔP	pressure drop (Pa)
Q	heat transfer rate (W)
u_{in}	inlet velocity (m s)
T	temperature (K)
ΔT	temperature difference (K)
ΔT_{max}	maximum temperature difference (K)
ΔT_{min}	minimum temperature difference (K)
ΔT_m	logarithmic mean temperature difference
Greek symbols	
λ	thermal conductivity (W m^{-1} K^{-1})
μ	dynamic viscosity (kg m^{-1} s^{-1})
ρ	density (kg m^3)
φ	volume fraction
Subscripts	
i, j	direction of coordinate
in	inlet
out	outlet
$wall$	wall
w	water
s	smooth helical coil
cr	critical
nf	nanofluid
bf	base fluid
p	nanoparticles
Abbreviations	
3D	three-dimensional
HCTTE	helically coiled tube with twisted elliptical
TPF	Thermal Performance Factor

References

1. Sheikholeslami, M.; Jafaryar, M.; Abohamzeh, E.; Shafee, A.; Babazadeh, H. Energy and entropy evaluation and two-phase simulation of nanoparticles within a solar unit with impose of new turbulator. *Sustain. Energy Technol. Assess.* **2020**, *39*, 100727. [CrossRef]
2. Suri, A.R.S.; Kumar, A.; Maithani, R. Effect of square wings in multiple square perforated twisted tapes on fluid flow and heat transfer of heat exchanger tube. *Case Stud. Therm. Eng.* **2017**, *10*, 28–43. [CrossRef]
3. Sheikholeslami, M.; Soleimani, S.; Ganji, D. Effect of electric field on hydrothermal behavior of nanofluid in a complex geometry. *J. Mol. Liq.* **2016**, *213*, 153–161. [CrossRef]

4. Xu, P.; Yu, B.; Qiu, S.; Poh, H.J.; Mujumdar, A.S. Turbulent impinging jet heat transfer enhancement due to intermittent pulsation. *Int. J. Therm. Sci.* **2010**, *49*, 1247–1252. [CrossRef]
5. Al-Obaidi, A.R.; Chaer, I. Study of the flow characteristics, pressure drop and augmentation of heat performance in a horizontal pipe with and without twisted tape inserts. *Case Stud. Therm. Eng.* **2021**, *25*, 100964. [CrossRef]
6. Gómez-Villarejo, R.; Estellé, P.; Navas, J. Boron nitride nanotubes-based nanofluids with enhanced thermal properties for use as heat transfer fluids in solar thermal applications. *Sol. Energy Mater. Sol. Cells* **2020**, *205*, 110266. [CrossRef]
7. Lin, W.; Shi, R.; Lin, J. Heat Transfer and Pressure Drop of Nanofluid with Rod-like Particles in Turbulent Flows through a Curved Pipe. *Entropy* **2022**, *24*, 416. [CrossRef]
8. Tusar, M.; Noman, A.; Islam, M.; Yarlagadda, P.; Salam, B. CFD study of heat transfer enhancement and fluid flow characteristics of turbulent flow through tube with twisted tape inserts. *Energy Procedia* **2019**, *160*, 715–722. [CrossRef]
9. Khan, M.I.; Waqas, M.; Hayat, T.; Alsaedi, A. Behavior of stratification phenomenon in flow of Maxwell nanomaterial with motile gyrotactic microorganisms in the presence of magnetic field. *Int. J. Mech. Sci.* **2017**, *131–132*, 426–434. [CrossRef]
10. Naphon, P.; Wiriyasart, S.; Prurapark, R.; Srichat, A. Numerical study on the nanofluid flows and temperature behaviors in the spirally coiled tubes with helical ribs. *Case Stud. Therm. Eng.* **2021**, *27*, 101204. [CrossRef]
11. Khoshvaght-Aliabadi, M.; Tavasoli, M.; Hormozi, F. Comparative analysis on thermal–hydraulic performance of curved tubes: Different geometrical parameters and working fluids. *Energy* **2015**, *91*, 588–600. [CrossRef]
12. Ali, M.A.; Sajid, M.; Uddin, E.; Bahadur, N.; Ali, Z. Numerical Analysis of Heat Transfer and Pressure Drop in Helically Micro-Finned Tubes. *Processes* **2021**, *9*, 754. [CrossRef]
13. Khoshvaght-Aliabadi, M.; Feizabadi, A. Compound heat transfer enhancement of helical channel with corrugated wall structure. *Int. J. Heat Mass Transf.* **2020**, *146*, 118858. [CrossRef]
14. Promthaisong, P.; Jedsadaratanachai, W.; Eiamsa-Ard, S. 3D Numerical study on the flow topology and heat transfer characteristics of turbulent forced convection in spirally corrugated tube. *Numer. Heat Transf. Part A Appl.* **2016**, *69*, 607–629. [CrossRef]
15. Xin, R.C.; Ebadian, M.A. The Effects of Prandtl Numbers on Local and Average Convective Heat Transfer Characteristics in Helical Pipes. *J. Heat Transf.* **1997**, *119*, 467–473. [CrossRef]
16. Yu, C.; Zhang, H.; Wang, Y.; Zeng, M.; Gao, B. Numerical study on turbulent heat transfer performance of twisted oval tube with different cross sectioned wire coil. *Case Stud. Therm. Eng.* **2020**, *22*, 100759. [CrossRef]
17. Promvonge, P.; Eiamsa-Ard, S. Heat transfer behaviors in a tube with combined conical-ring and twisted-tape insert. *Int. Commun. Heat Mass Transf.* **2007**, *34*, 849–859. [CrossRef]
18. Thianpong, C.; Eiamsa-Ard, P.; Wongcharee, K.; Eiamsa-Ard, S. Compound heat transfer enhancement of a dimpled tube with a twisted tape swirl generator. *Int. Commun. Heat Mass Transf.* **2009**, *36*, 698–704. [CrossRef]
19. Gkountas, A.A.; Benos, L.T.; Nikas, K.-S.; Sarris, I.E. Heat transfer improvement by an Al_2O_3-water nanofluid coolant in printed-circuit heat exchangers of supercritical CO_2 Brayton cycle. *Therm. Sci. Eng. Prog.* **2020**, *20*, 100694. [CrossRef]
20. Schmidt, E.F. Wärmeübergang und Druckverlust in Rohrschlangen. *Chem. Ing. Tech.* **1967**, *39*, 781–789. [CrossRef]
21. Srinivasan, P.; Nandapurkar, S.; Holland, F. Friction factors for coils. *Trans. Inst. Chem. Eng. Chem. Eng.* **1970**, *48*, T156–T161.
22. Ho, M.X.; Pan, C. Experimental investigation of heat transfer performance of molten HITEC salt flow with alumina nanoparticles. *Int. J. Heat Mass Transf.* **2017**, *107*, 1094–1103. [CrossRef]
23. Salimpour, M.R. Heat transfer coefficients of shell and coiled tube heat exchangers. *Exp. Therm. Fluid Sci.* **2009**, *33*, 203–207. [CrossRef]
24. Yanase, S.; Goto, N.; Yamamoto, K. Dual solutions of the flow through a curved tube. *Fluid Dyn. Res.* **1989**, *5*, 191–201. [CrossRef]
25. Itō, H. Friction Factors for Turbulent Flow in Curved Pipes. *J. Basic Eng.* **1959**, *81*, 123–132. [CrossRef]
26. Moawed, M. Experimental study of forced convection from helical coiled tubes with different parameters. *Energy Convers. Manag.* **2011**, *52*, 1150–1156. [CrossRef]
27. Pawar, S.; Sunnapwar, V.K. Experimental studies on heat transfer to Newtonian and non-Newtonian fluids in helical coils with laminar and turbulent flow. *Exp. Therm. Fluid Sci.* **2013**, *44*, 792–804. [CrossRef]